Genome analysis of Parmales, a sister group of diatoms, reveals the evolutionary specialization of diatoms from phago-mixotrophs to photoautotrophs

Hiroki Ban[1], Shinya Sato[2], Shinya Yoshikawa[2], Kazumasa Yamada[2], Yoji Nakamura[3], Mutsuo Ichinomiya[4], Naoki Sato[5], Romain Blanc-Mathieu[1,6], Hisashi Endo[1], *Akira Kuwata[7], *Hiroyuki Ogata[1]

Affiliations:

1. Bioinformatics Center, Institute for Chemical Research, Kyoto University, Gokasho, Uji, Kyoto, 611-0011, Japan
2. Department of Marine Science and Technology, Fukui Prefectural University, 1-1 Gakuen-cho, Obama City, Fukui 917-0003, Japan
3. Bioinformatics and Biosciences Division, Fisheries Stock Assessment Center, Fisheries Resources Institute, Japan Fisheries Research and Education Agency, 2-12-4 Fuku-ura, Kanazawa, Yokohama, Kanagawa 236-8648, Japan
4. Prefectural University of Kumamoto, 3-1-100 Tsukide, Kumamoto 862-8502, Japan
5. Graduate School of Arts and Sciences, University of Tokyo, Komaba, Meguro-ku, Tokyo 153-8902, Japan
6. Laboratoire de Physiologie Cellulaire & Végétale, CEA, Univ. Grenoble Alpes, CNRS, INRA, IRIG, Grenoble, France
7. Shiogama field station, Fisheries Resources Institute, Japan Fisheries Research and Education Agency, 3-27-5 Shinhama-cho, Shiogama, Miyagi, Japan

Corresponding author:

A. Kuwata, E-mail: akuwata@affrc.go.jp, Phone: +81-22-365-9929

H. Ogata, E-mail: ogata@kuicr.kyoto-u.ac.jp, Phone: +81-774-38-3270

Abstract

The order Parmales (Bolidophyceae) is a minor group of pico-sized eukaryotic marine phytoplankton that contains species with cells surrounded by silica plates. Previous studies revealed that Parmales is a member of ochrophytes and sister to diatoms (Bacillariophyta), the most successful phytoplankton group in the modern ocean. Therefore, parmalean genomes can serve as a reference to elucidate both the evolutionary events that differentiated these two lineages and the genomic basis for the ecological success of diatoms vs. the more cryptic lifestyle of parmaleans. Here, we compared the genomes of eight parmaleans and five diatoms to explore their physiological and evolutionary differences. Parmaleans were predicted to be phago-mixotrophs. By contrast, diatoms have undergone loss of genes related to phagocytosis, indicating the ecological specialization from phago-mixotroph to photoautotroph in the early evolution of diatoms. Furthermore, diatoms showed significant enrichment in gene sets involved in silica metabolism, nutrient uptake capacity, carbon concentrating mechanisms, and iron uptake in comparison with parmaleans. Overall, our results suggest a strong evolutionary link between the loss of phago-mixotrophy and specialization to a silicified photoautotrophic life stage early in diatom evolution after diverging from the Parmales lineage.

Introduction

Parmales is a group of pico-sized (2–5 μm) eukaryotic marine phytoplankton with cells surrounded by silicified plates[1]. Parmaleans are widespread in the ocean, from polar to subtropical regions, and are relatively abundant in polar and subarctic regions. Parmalean sequences are most abundant in the picoplanktonic fraction (0.8–5 μm) of the global ocean metabarcoding data from *Tara* Oceans and represent at most 4% of the sequences of photosynthetic organisms and less than 1% on average[2]. Currently, only 17 taxa of parmaleans have been described[3,4]. SEM and TEM observations, molecular phylogenetics, and photosynthetic pigment analyses indicated that Parmales belongs to ochrophytes (class Bolidophyceae)[5] and is the sister taxon of diatoms (phylum Bacillariophyta). Bolidophyceae also contains pico-sized photosynthetic naked flagellates (called bolidomonads) that mainly inhabit subtropical waters[6]. Recent phylogenetic analyses using several newly isolated strains revealed that flagellated bolidomonad species belong to the silicified and non-flagellated parmalean genus *Triparma* within Bolidophyceae, suggesting that the *Triparma* life cycle switches between silicified/non-flagellated and naked/flagellated stages[2].

Diatoms are the most successful phytoplankton group in the modern ocean; they have high diversity (ca. 10^5 species[7]) and high primary productivity, contributing an estimated 20% of photosynthesis on Earth. Diatoms are thought to be particularly successful in dynamic environments such as upwelling areas, and it has been suggested that their ecological success is supported by traits such as silicified cell wall defense[8] and luxury nutrient uptake[9]. However, despite advances in understanding diatom genomes during the last two decades, the reasons underlying the success of diatoms in modern oceans remain poorly understood. To understand the ecological success of diatoms, characterization of the evolution of physiology-related genes in this taxon is necessary.

Although parmaleans are the closest relatives of diatoms, they show much lower biomass, species diversity, and ecological impact than their sister taxon. The proposed parmalean life cycle, which switches between silicified/non-flagellated and naked/flagellated stages, is similar to the proposed origin of diatoms[2]. Ancestral diatoms were possibly haploid flagellates that formed silicified diploid zygotes[10]. The mitotic division of the zygote might have taken place preferentially to give rise to centric diatoms[11], which is the most ancient diatom group with a diploid vegetative stage producing naked flagellated haploid male gametes for sexual reproduction[12]. Thus, a comparison of parmaleans and diatoms is expected to provide important clues on differences in

76 their ecological strategies and evolutionary paths. To date, only limited genomic data on
77 parmaleans have been available[13], and the genomic features and evolutionary events that led to
78 differences between them and diatoms have remained unstudied. In this study, we generated seven
79 novel parmalean genome assemblies. These seven draft genomes, one previously determined
80 parmalean genome, and five publicly available diatom genomes were used to perform a
81 comparative genome analysis. Our results delineate the evolutionary trajectories of these two
82 lineages after their divergence and correlate their differential ecological features with their
83 genomic functions.

Results and Discussion

General genomic features

In this study, we obtained whole-genome sequences of seven parmaleans, including six strains from two genera (*Triparma* and *Tetraparma*) that are frequently observed in the subarctic Pacific Ocean[4,14], as well as one strain from an undescribed taxon that is phylogenetically and morphologically distinct from known parmaleans (hereafter referred to as 'Scaly parma', Sato et al. in prep.). Together with the previously sequenced *Triparma laevis* f. *inornata* genome[13], we built a database of eight parmalean strain genomes. The parmalean genomes were similar in size, ranging from 31.0 Mb for 'Scaly parma' to 43.6 Mb for *Tetraparma gracilis* (Table 1). The predicted numbers of genes ranged from 12,177 for 'Scaly parma' to 16,002 for *Triparma laevis* f. *longispina* (Table 1). These genome sizes are relatively constant compared to diatom genomes and similar to those of *Thalassiosira pseudonana* (32.4 Mb)[15] and *Phaeodactylum tricornutum* (27.4 Mb)[16], which have rather small genomes among diatoms.

Analysis of orthologous groups (OGs) revealed 62,363 OGs among the parmaleans (8 strains), diatoms (5 strains), and other stramenopiles (5 strains). Phylogenomic analysis based on 164 single-copy OGs clearly shows parmaleans are monophyletic and sister to diatoms (Fig. 1a). 34,292 OGs were present only in diatoms or parmaleans and not in other stramenopiles (Fig. 1b: yellow + orange + purple + green in diatoms and Parmales). Of those, only 1,448 OGs were shared by diatoms and parmaleans (Fig. 1b: yellow). 20,974 OGs were specific to diatoms (diatom-specific OGs, Fig. 1b: orange + green in diatoms), and 11,870 OGs were specific to parmaleans (Parmales-specific OGs, Fig. 1b: purple and green in Parmales). 99.7% of the genes in the core OGs conserved in all analysed strains (1,153 OGs, Fig. 1b: red) had InterPro domains, and 77.1% of the genes in the OGs shared only by diatoms and parmaleans (1,448 OGs, Fig. 1b: yellow) had InterPro domains. By contrast, only 24.9% of genes in diatom-specific OGs (20,974 OGs, Fig. 1b: orange + green in diatoms) and 55.1% of genes in parmalean-specific OGs (11,870 OGs, Fig. 1b: purple and green in Parmales) had InterPro domains. These results reveal that many lineage-specific genes are functionally unknown.

Differentially enriched protein domains

By comparing the eight parmalean and five diatom genomes, we found 64 and 315 InterPro domains in which the diatom and Parmales lineages, respectively, were significantly enriched. Cyclin domains and heat-shock transcription factor domains in which diatoms are enriched have been known to exhibit expanded gene families compared with other eukaryotes[16,17] (Fig. 2a). In addition, diatoms were enriched in protease domains and sulfotransferase domains. Serine proteases and metalloproteases are known to be induced by limitations of nitrogen, iron, silicon, and light[18,19]. Sulfotransferase is an enzyme that catalyses sulfonation and is thought to be related to programmed cell death in *Skeletonema marinoi*, a bloom-forming marine diatom[20]. These gene families are thought to be related to the stress response process in diatoms.

InterPro domains in which parmaleans were enriched included those involved in intracellular signalling pathways, such as the G protein signalling, cyclic nucleotide signalling, calcium signalling, and action potential pathways (Fig. 2a). G protein-coupled receptors were involved in responses to sexual cues in the planktonic diatom *Pseudo-nitzschia multistriata*[17], and to colonization in *Phaeodactylum tricornutum,* a planktonic diatom that also has a benthic morphotype[21]. Diatoms also exhibit action potential signalling to modulate their cellular motility[22,23]. Furthermore, parmaleans encode a strikingly greater number of calcium-binding proteins (up to 300) that could act as messenger molecules[24] (Fig. 2b). Enrichment of intracellular signalling pathways in parmaleans may be associated with their putative alternating life cycle stages (i.e., silicified/non-flagellated and naked/flagellated cell stages[2]).

Parmalean genomes were notably enriched in domains associated with lipids and fatty acids (Fig. 2a). For example, diacylglycerol acyltransferase is an enzyme for the terminal step in the production of triacylglycerol, the main component of stored lipids[25]. The steroidogenic acute regulatory protein-related lipid transfer (START) domain that binds to lipids and sterols[26] is one of the domains in which parmalean genomes are most enriched, with up to 174 domains in *Tetraparma gracilis*. This domain sometimes consists of multi-domain proteins and works in lipid trafficking, lipid metabolism, and cell signalling in animals and land plants[26]. START domain-containing proteins in parmaleans also contain other functional domains, such as lipid metabolism enzymes, transporters, kinases, and transcription factors (Fig. 2c). These results suggest diverse lipid-related physiological processes in parmaleans.

Phagotrophy

Some InterPro domains in which parmaleans are enriched are known to be involved in phagotrophy[27], including cell adhesion[28], intercellular signalling (e.g., small GTP-binding proteins such as Rho)[29], cytoskeleton[30], lysosome[31], and WASH[32] (WASP and SCAR homolog) complex proteins (Fig. 2d). Specific genetic markers of phagotrophy are not known, but parmaleans were predicted as phago-mixotrophs (high scores > 0.98) according to a gene-based phago-mixotrophy prediction model[27], whereas diatoms were not (low scores < 0.07) (Fig. 2e). This result suggests that parmaleans are capable of phagocytosis. We also applied this prediction model to the bolidomonads (naked/flagellated parmaleans) transcriptomes, and bolidomonads were also predicted as phago-mixotrophs (high scores > 0.98, Fig. 2e). Although there is no experimental evidence of phagocytosis in silicified parmaleans, a field study demonstrated that bolidomonads feed on cyanobacteria[33,34]. As transcriptome data reflect gene repertoires expressed under specific physiological conditions, bolidomonads might be phagotrophic. It remains unclear which life cycle stages of the parmaleans that we analysed are phagotrophic. However, assuming that bolidomonads indeed represent a part of the parmalean life cycle[3], and a possibility that the silicified parmalean cell wall could physically interfere with feeding bacteria, it is likely that parmaleans perform phagocytosis in their putative naked/flagellated stage (Fig. 2f).

In the following sections, we move from the analysis of enriched domains to more focused investigation of genes in specific pathways and functions.

Flagellum

To investigate the possibility that parmaleans can produce a flagellated cell[2], we searched for genes responsible for flagellar motility (i.e., intraflagellar transport (IFT) subunit genes[35] [IFT-A complex (6 genes), IFT-B complex (15 genes), BBSome (7 genes)]) in the parmalean and diatom genomes and bolidomonad transcriptomes. Flagellum structural genes for tubulin, radial spokes, dynein arms, and the central pair complex were excluded from analysis because these genes are also involved in other processes/structures (such as the centriole in *Triparma laevis*[36]) and are not unique to the flagellum. For this analysis, bolidomonad transcriptomes and centric diatom genomes were considered as positive controls because of the presence of the flagellar structure[6] and the presence of flagellated sperm in their life cycle[37], respectively. Similarly, pennate diatom

174 genomes were considered as negative controls because flagellar structures have never been
175 observed in this group, despite the accumulated knowledge concerning sexual reproduction[38].
176 A nearly-full set of the flagellar genes were found in parmalean genomes and bolidomonad
177 transcriptomes, whereas IFT-A and BBsome were completely absent in both types of diatoms (Fig.
178 2g). IFT-B was partially lost in centric diatoms and completely lost in pennate diatoms. These
179 results suggest that parmaleans have a flagellated stage in their life cycle and are consistent with
180 the idea that parmaleans are phago-mixotrophic in their putative naked/flagellated stage. Jensen et
181 al.[39] speculated that the two central microtubules were dispensed with in sperms of centric diatoms.
182 Given the detection of the nearly-full set of flagellar genes in the parmaleans vs. the complete lack
183 of IFT-A and BBSome and partial loss of IFT-B in the centric diatoms, it is possible that
184 evolutionary pressure to maintain the flagellated stage is higher in parmaleans than in centric
185 diatoms (e.g., because of the presence of a frequent or prolonged flagellated stage in parmaleans,
186 which is not expected for sperms of centric diatoms).
187
188 **Nitrogen metabolism**
189 The number of transporter genes involved in the uptake of nitrogen sources differed greatly
190 between diatoms and parmaleans (Fig. 3a). Parmaleans had 1–3 nitrate/nitrite transporter genes,
191 whereas diatoms had 4–9. Only one urea transporter gene was present in each parmalean, whereas
192 3–6 genes were present in each diatom. Diatoms tended to have more ammonia transporter genes
193 than parmaleans, although the difference was not as obvious as for the other transporters (1–4
194 genes for parmaleans vs. 3–8 for diatoms). Genes for the vacuolar nitrate transporter, which stores
195 nitrogen sources in the vacuole[40], were absent from parmalean genomes. This suggests that
196 parmaleans may be less competent to store nitrogen sources than diatoms, although the possibility
197 that parmaleans encode another non-homologous vacuolar nitrate transporter is not excluded.
198 Parmaleans had all of the ornithine–urea cycle genes, as with diatoms[15] and other
199 stramenopiles[41] (Fig. 3b, Supplementary Fig. 2). Other involved genes (i.e., those encoding
200 NAD(P)H nitrite reductase, carbamate kinase, formamidase, cyanate lyase, and hydroxylamine
201 reductase) were present in diatoms but absent from parmaleans. NAD(P)H nitrite reductase is a
202 major enzyme in nitrogen metabolism that catalyses production of ammonia from nitrite.
203 Carbamate kinase is a major enzyme that produces carbamoyl phosphate, which is a precursor of
204 the urea cycle. In contrast to this difference, both parmaleans and diatoms encode alternative

enzymes for these proteins, namely ferredoxin-nitrite reductase and carbamoyl phosphate synthetase, having the same functions as NAD(P)H nitrite reductase and carbamate kinase, respectively. Therefore, parmalean nitrogen metabolism likely relies on the latter set of enzymes, while diatoms may have more efficient nitrogen metabolism by possessing multiple sets of enzymes. Formamidase, cyanate lyase, and hydroxylamine reductase function around the main pathway of nitrogen metabolism. Previous studies showed that formamidase and cyanate lyase are upregulated under N-limited conditions in *Aureococcus anophagefferens*[42] and *P. tricornutum*[43]. Diatoms encoding these enzymes may have the ability to obtain ammonia from intercellular nitrogen compounds even when they cannot obtain extracellular nitrogen[42,43]. By contrast, parmaleans lacking these enzymes may not have this capacity.

Iron metabolism

Iron acts as an electron carrier in the photosynthesis system and various metabolic processes in phototrophs. In marine ecosystems, iron is one of the prime limiting elements for phototrophs because of high demand[44]. Therefore, iron uptake ability is an important factor for competition in marine environments. We searched for iron metabolism-related genes in diatom and parmalean genomes. Ferric reductase (FRE), a high-affinity reductive iron uptake system component, was found in all diatoms and parmaleans investigated (Fig. 3c), but parmaleans completely lacked Fe^{3+} permease (FTR) genes (Fig. 3c). Parmalean genomes encoded genes with high sequence similarity to diatom FTR genes, but the parmalean sequences lacked the [REXXE] motif, which is important for iron permeation[45]. This indicates that the diatom/Parmales common ancestor possessed FTR but parmalean FTR homologs may have lost their ability to enable iron permeation during evolution. As for the genes involved in the non-reductive iron uptake system, iron starvation-induced protein 2 (ISIP2)[46] was widely distributed in parmaleans, whereas ISIP1 was not present (Fig. 3c). ISIP1 plays an important role in siderophore uptake in diatoms and is considered a highly efficient iron uptake gene[47]. Our results support the idea that ISIP1 is a diatom-specific gene[47] and its presence may underlie diatoms' high iron uptake capacity.

Most parmaleans encode genes for plastocyanin, a copper-containing redox protein that can substitute for cytochrome c_6, which is a redox protein that requires iron and transfers electrons from the cytochrome b_6–f complex to photosystem I during photosynthesis. It was generally thought that chlorophyll *c*-containing algae lack plastocyanin, but several pelagic diatoms from

different genera (including *Thalassiosira oceanica*) encode plastocyanin and are thought to be adapted to iron-deficient pelagic regions[48,49]. Parmaleans may also have an environment-dependent adaptive strategy to differentially use cytochrome c_6 and plastocyanin. Phylogenetic analysis revealed that the plastocyanin genes from diatoms and parmaleans were monophyletic (with dictyochophytes and others), except for *Fragilariopsis kerguelensis,* which was grouped with bacteria (Supplementary Fig. 3). This result is inconsistent with the previously proposed horizontal acquisition of plastocyanin genes in pelagic diatoms[48]. The diatom/Parmales common ancestor likely possessed both cytochrome c_6 and plastocyanin, and some diatoms (mostly coastal ones) lost their plastocyanin (Fig. 3d).

Silicate metabolism

Each parmalean genome contained at most one silicic acid transporter (SIT) gene, whereas diatom genomes contained multiple SIT genes (Fig. 3a). Most SIT genes of diatoms and 'Scaly parma' encode a 10-fold transmembrane type (i.e., single SIT domain), whereas the SIT genes of the other parmaleans encode a 20-fold transmembrane type (i.e., two SIT domains). Phylogenetic analysis of SIT domains indicated that parmalean SIT genes belong to the most basal clade of diatom SITs (clade B)[50], and that the 20-fold transmembrane-type SITs of Parmales are the result of multiple (likely two times) domain duplications in the *Triparma* lineage (Fig. 4). A large number of paralogous SITs (at least five clades) in diatoms was generated through multiple gene duplications in the diatom lineage after it diverged from the Parmales lineage.

Silicanin homologs, some of which are biosilica-associated proteins[51], were found in Parmales. The parmalean genomes encoded 1–2 silicanin homologs, whereas the diatom genomes encoded 7–14 homologs. Parmalean silcanin homologs have the RXL domain, which is typical of many diatom biosilica-associated proteins[52–55] but lack the NQ-rich domain that is found in Sin1 and Sin2 of *Thalassosira pseudonana*[51]. Silicanin homologs are not known in other stramenopiles, but have been reported in transcriptome data of other non-diatom eukaryotes such as the ciliate *Tiarina fusus* and the dinoflagellate *Rhizochromulina marina*[51]. These silicanin homologs were found to be highly similar to those of the diatoms *Synedropsis recta* and *Thalassiosira weissflogii*, respectively (blastp search against the MMETSP database; identities are 68.3% and 100%, respectively, and e-values are both 0.0), implying that these genes from non-diatom eukaryotes originated from diatoms (either through HGT or contamination). Thus, the silicanin homologs

found in parmaleans are the first examples of non-horizontally transferred silicanin homologs in non-diatom species, implying that the silicanin gene was already present in the diatom/Parmales common ancestor. Silicanins, like SITs, have undergone multiple gene duplications within the diatom lineage after the diatom/Parmales divergence. Interestingly, SIT and silicanin proteins were not found in any bolidomonad transcriptomes, consistent with their lack of silica plates.

Ecological strategies and evolutionary scenarios

By comparing the genomes of eight parmaleans and five diatoms, we were able to delineate differences and similarities in gene content between these two taxa (Fig. 5). Based on the gene-based trophic model, our analysis suggests that parmaleans are phago-mixotrophs that can acquire nutritional resources such as carbon, nitrogen, phosphorus, vitamins, and trace elements (e.g., iron) by grazing other organisms, such as bacteria. Although phago-mixotrophs would be less dependent on inorganic nutrient resources, this advantage is traded off with an associated increase in metabolic costs for incorporating and maintaining the cellular components required for both autotrophy and phagotrophy. In addition, since phagotrophy reduces the cell surface area for transporter sites, phago-mixotrophs are thought to have lower growth efficiency relative to photoautotrophic specialists[56,57]. According to a theoretical study, mixotrophy is beneficial especially in oligotrophic water, whereas autotrophy is advantageous in eutrophic environments[58,59].

Previous studies suggested that some mixotrophs can widen their niche by alternating their trophic strategies[60,61]. For example, several coccolithophores (Haptophyta) are known to alternate between a motile phago-mixotrophic haploid stage and a non-motile autotrophic diploid stage based on nutrient condition[62]. Based on these facts and other field data, it has been previously hypothesized that parmaleans have a similar life stage alternation[3]. Namely, parmaleans may live as silicified photoautotrophs during winter (the cold mixing season) when nutrients are rich, while they may feed on bacteria through phagocytosis as naked flagellates during summer (the warm stratified season) when nutrients are depleted. Our study reinforces the possibility of such a life cycle in Parmales, by detecting the genes for phagocytosis which has a potential association with the naked-flagellate stage.

In addition to the absence of phagotrophy in diatoms, our analysis revealed a marked contrast in the gene repertoires between diatoms and parmaleans, with all indicating the

autotrophic adaptations of diatoms. For example, there is a large difference in the number of nutrient transporter genes between diatoms and parmaleans (Fig. 3a), clearly representing an adaptation of diatoms to eutrophic environments, although it is not clear whether these paralogous genes have different functions (e.g., affinity, transport rates, and subcellular localization) or a dosage effect[63]. In addition, there are differences in the number of genes involved in biophysical CCMs (Supplementary Fig. 4; See Supplementary Note). Diatoms possess higher CO_2 fixation capacity relative to other phytoplankton groups[64], and these gene repertoires may support this trait. We also revealed the expansion of protease and sulfotransferase genes in diatoms in addition to the previously described expansion of cyclin and heat-shock protein genes[16,17] (Fig. 2a). These genes are likely involved in stress response and population control, which support the extraordinary growth capacity of diatoms.

Most diatoms are photoautotrophs, and all diatoms that we studied were predicted as such (Fig. 2d, e). However, phagotrophy must have existed for the ancestor of diatoms to take up red algae as endosymbionts (i.e., secondary plastids). Some members of ochrophyte, such as chrysophytes and dictyochophytes[65], are known to be phago-mixotrophic. Our results suggest that Parmales, which is the closest group to diatoms, is also phago-mixotrophic. Thus, the diatom/Parmales common ancestor was firmly inferred as phago-mixotrophic, and there were massive serial gene loss events related to phagocytosis loss and specialization to photoautotrophy in the early evolution of diatoms after diverging from Parmales (ca. 180–240 million years ago[66]).

Diatoms always have silicified cell walls in the vegetative stage, whereas parmaleans putatively switch between two life stages, silicified/non-flagellated and naked/flagellated stages. The silicified cell wall provides a barrier against grazers, parasites, and pathogens[67], but is obviously incompatible with phagocytosis as it completely covers the cell. Thus, there is a trade-off between silicification/autotrophy and phagocytosis, and the loss of phagotrophy in diatoms may have been related to benefits from the silicified cell wall. To reveal why photoautotrophic diatoms diverged from the phago-mixotrophic lineage and specialized to the silicified life stage, it is necessary to understand not only the costs and benefits associated with mixotrophy but also those of defence by silicified cell walls.

The next possible step in the evolution of diatoms after specialization to silicification and photoautotrophy might have been to thicken their silicified cell wall and increase their cell size[8]. Diatoms tend to have larger cell sizes than parmaleans, and the evolution of these traits has the

great advantage of increasing resistance to grazers. The evolution of silicic acid transporter genes (Fig. 4) may have supported the evolution of silicified cell walls because diatoms with thick walls and large cells require large amounts of silicate. It is also known that nutrient metabolism, especially nitrogen metabolism, is closely related to silica deposition in diatoms[68]. Thus, the ability of diatoms to take up nutrients may also be related to the evolution of their silicified cell wall. Silicanin, which diversified in diatoms, may have been important in the precise control of the formation of thick cell walls. It has been also pointed out that vacuoles play a major role in cell size expansion[8]. However, there is little evidence of differences in vacuole-related genes between parmaleans and diatoms (e.g., lack of a vacuolar nitrate transporter homolog in parmaleans), so further discovery and analysis of the relevant genes are needed to address this issue.

Diatoms are also an important group in iron usage in the ocean, often dominating iron-stimulated blooms[69]. Analyses of iron utilization strategies revealed that the ISIP1 gene, which is involved in siderophore-mediated iron acquisition, is absent in parmaleans and unique to diatoms (Fig. 3c). Siderophores are thought to be major components of microbial iron cycling in the ocean[70]. The lack of the ISIP1 gene in parmaleans supports the idea that this gene underlies the high iron uptake capacity of diatoms and supports their photoautotrophic lifestyle. We also found that plastocyanin, which is an alternative for iron-requiring proteins in photosynthesis, is widely distributed in parmaleans. Phylogenetic analysis suggests that each lineage of diatoms lost their plastocyanin genes independently, and that pelagic diatoms and parmaleans conserved plastocyanin genes from their common ancestor (Fig. 3d). Parmaleans retained plastocyanin to balance their restricted capacity for iron uptake in iron-limited environments; diatoms increased their iron uptake capacity (e.g., ISIP1), while several lineages have specialized to coastal eutrophic environments and lost plastocyanin.

Our analysis also revealed that the ornithine–urea cycle, the mitochondrial pay-off phase of the glycolytic pathway, and the Entner–Doudoroff pathway, which have been cited as unique features of diatoms, were substantially conserved from common ancestor of Parmales and diatoms (Fig. 3b, Fig. 5, Supplementary Fig. 2, Supplementary Fig. 5: see Supplementary Note). We also found the expansion of genes related to lipid metabolism and intracellular signalling, and the degenerative evolution of several genes related to iron uptake and ornithine–urea metabolism in Parmales (see Supplementary Note). However, their physiological functions and evolutionary

359 significances remain unclear. Future studies based on a larger set of genomic data will further
360 enhance understanding of the physiology, ecology, and evolution of these fascinating organisms.

Methods

Culture

We used strains of the parmaleans *Triparma laevis* f. *inornata* (NEIS-2656), *Triparma laevis* f. *longispina* (NIES-3700), *Triparma verrucosa* (NIES-3699), and *Triparma strigata* (NIES-3701), isolated from the Oyashio region of the western North Pacific. For the other strains, water samples were collected at 10 m in the Notoro-ko lagoon (44º3'2.1" N, 144º9'38.8" E, December 2015) for *Triparma retinervis*, at 10 m in the Sea of Okhotsk (45º25'0" N, 145º10'0" E, June 2017) for *Tetraparma gracilis* and *Triparma columacea*, and at 30 m in the Sea of Okhotsk (44º30'0" N, 144º20'0" E, June 2014) for the uncharacterized 'Scaly parma'. The strains were isolated by serial dilution with siliceous cell wall labelling techniques described previously[5]. The strains were cultured in f/2 medium[71] at 5 °C under a light intensity of ca. 30 µmol photons m^{-2} s^{-1} (14:10 L:D cycle).

Genomic DNA, RNA extraction and sequencing

Cells grown under exponential growth phase were harvested by centrifugation, and either DNA (all strains, except *Triparma laevis* f. *inornata*) or RNA (for *Triparma laevis* f. *inornate, Triparma strigata, Triparma retinervis* and 'Scaly parma') was extracted using the DNeasy Plant Mini Kit or RNeasy Plant Mini Kit (Qiagen, Venlo, Netherlands), respectively. Libraries were generated using the Illumina TruSeq DNA/RNA sample preparation kit (Illumina, Inc., San Diego, USA). Sequencing of whole genomes or transcriptomes was performed on an Illumina HiSeq X (150 bp, paired-end) or HiSeq 2000 (100 bp, paired-end), respectively. Exceptionally, the genome of *Triparma laevis* f. *longispina* and 'Scaly parma' was sequenced with an Illumina HiSeq 2500 (150 bp, paired-end). DNA extraction and sequencing methods for *Triparma laevis* f. *inornate* were already reported in Kuwata et al[13].

Genome assembly and microbial sequence contamination removal

Genome assembly and contamination removal methods for *Triparma laevis* f. *inornate* were already reported in Kuwata et al[13]. For the other strains, the Illumina reads were trimmed with Trimmomatic (v.0.38)[72] using the following parameters: LEADING:20 TRAILING:20 SLIDINGWINDOW:4:15 MINLEN:36 TOPHRED33. The filtered reads were assembled by

391 Platanus (v.1.2.4)[73] with default options. To remove bacterial contamination from contigs,
392 clustering of contigs was performed based on the coverage calculated by read mapping, GC
393 frequency, and k-mer frequency. In addition, the phylogenetic classification of the genes in the
394 contigs was estimated using lowest common ancestor analysis. The results were used to determine
395 the clusters composed of bacterial contigs. Read mapping to assembled contigs with the filtered
396 reads was performed with BWA (v.0.7.17)[74]. The coverage was calculated from the resulting .sam
397 file using a custom-written Perl script, which was also used to determine the GC content. The
398 tetramer frequency of contigs was calculated using cgat (v.0.2.6)[75]. Open reading frames (ORFs)
399 were predicted using GeneMarkS (v.4.30)[76] and their taxonomy was annotated with a last common
400 ancestor strategy as in Carradec et al[77]. ORFs were searched against a database composed of
401 UniRef 90[78], MMETSP database[79], and Virus-Host DB[80] using DIAMOND (v.0.9.18)[81]. Selected
402 hits were then used to derive the last common ancestor of the query ORFs with the NCBI taxonomy
403 database. Clustering of contigs was performed using the R script provided in the CoMet
404 workflow[82] with coverage, GC content, and k-mer frequency as information sources. The organism
405 from which each cluster originated was determined from the estimated phylogeny of the genes in
406 the contigs belonging to the cluster. Contigs belonging to bacterial-derived clusters were excluded
407 from the datasets and not used in downstream analyses.
408 We also performed a blastn (v.2.11.0) search against the organelle genomes of *Triparma*
409 *laevis* f. *inornata*[83] to remove the organelle genome from assembled contigs. Contigs that hit the
410 organelle genome of *T. laevis* f. *inornata* with E-values < 1e−40 were excluded from our dataset
411 as organelle genomes.
412
413 **Genome annotations**
414 For *T. laevis* f. *inornata* genome[13], rRNA and tRNA genes were predicted by Barrnap
415 (v.0.6, http://www.vicbioinformatics.com/software.barrnap.shtml) and tRNA-scan-SE (v.1.23)[84],
416 respectively. The protein coding-genes were predicted by AUGUSTUS (v.3.2.2)[85] with the RNA-
417 seq data mentioned above. First, the RNA-seq reads processed by fastx-toolkit (v.0.0.13,
418 http://hannonlab.cshl.edu/fastx_toolkit/) were mapped to the contig of *T. laevis* f. *inornata* nuclear
419 genome and assembled into transcript contigs using Tophat (v.2.1.1)[86], Cufflinks (v.2.2.1)[87] and
420 Trinity (v.2.0.6)[88], respectively. The diatom protein sequences from *Thalassiosira pseudonana*[15]
421 and *Phaeodactylum tricornutum*[16] were subsequently aligned to the transcript contigs using tblastn

search (v.2.2.29) and Exonerate (v.2.4.0)[89] for detecting CDS regions in the *T. laevis* f. *inornata* genome. Finally, a total of 687 loci on the *T. laevis* f. *inornata* contigs were selected as those carrying full-length CDSs and used for parameter fitting in training hidden Markov models in AUGUSTUS. In gene prediction, the mapping data from both RNA-seq reads and diatom protein sequences were utilized as hints in AUGUSTUS.

For other genomes, tRNA genes were predicted using tRNAscan-SE (v.2.0.7)[90]. Non-coding RNAs excluding tRNAs but including rRNAs were predicted with the Rfam database using infernal (v.1.1.3)[91]. Repeats and transposable elements were annotated and soft-masked using RepeatModeler (v.2.0.1)[92] and RepeatMasker (v.4.1.0)[93]. For *Triparma strigata, Triparma retinervis* and 'Scaly parma', the protein-coding genes were predicted by BRAKER2[94] with the RNA-seq data mentioned above and a reference protein sequence database. We generated a reference protein sequence database for BRAKER2 from OrthoDB[95], MMETSP database[79] and *T. laevis* f. *inornata* protein sequences predicted previously. Firstly, RNA-seq data were mapped to the contigs by STAR (v.2.7.3a)[96], generating a .bam file. Secondly, BRAKER2 was run in –etpmode mode with the generated .bam file and the reference protein sequence database as the protein hints. For *Triparma laevis* f. *longispina*, *Triparma verrucosa*, *Triparma columacea* and *Tetraparma gracilis*, the protein-coding genes were predicted by BRAKER2 only with a reference protein sequence database. We updated the mentioned reference protein sequence database with the predicted protein sequences form *Triparma strigata*, *Triparma retinervis*, and 'Scaly parma', and generated a new database. Finally, BRAKER2 was run in -epmode using the newly generated reference protein sequence database as the protein hints.

Functional Annotation

For methodological consistency, we applied the same annotation pipelines for our novel genomes and the genomes downloaded from public databases. Genes were functionally annotated by InterProScan (v.5.26-65.0)[97] and eggNOG-Mapper (v.2.0.1)[98] with the eggNOG database (v.5.0)[99]. Protein localization was predicted using MitoFates (v.1.1)[100], TargetP (v.2.0)[101], SignalP (v.4.1)[102], and ASAFIND (v.1.1.7)[103]. Protein functions and localizations were manually curated for detailed analyses.

452 **Phylogenomic analysis**

453 Orthologous genes (OGs) were determined by OrthoFinder (v.2.3.7)[104] with protein
454 sequences of parmalean genomes, other available stramenopile genomes, and ochrophyte
455 transcriptomes (Supplementary Data 11) from the MMETSP database[79]. Only single-copy genes
456 in each OG and genes that were found in the 18 stramenopile species were retained for downstream
457 phylogenomic analysis, resulting in 164 OGs. Gene sequences within each OG were aligned using
458 MAFFT (v.7.453)[105] in the linsi mode, and poorly aligned regions from the multiple sequence
459 alignment were removed by trimAl (v.1.4.1)[106] in the automated1 mode. The resulting supermatrix
460 contained 50,707 amino acid positions for 18 species, with 5.85% missing data. A maximum
461 likelihood tree was inferred by RAxML (v.8.2.12)[107] with the partition information of each gene
462 and the LG + F model. We performed 1,000 bootstrap replicates and all bootstrap values were 100,
463 indicating full support.
464

465 **Gene family and protein domain analysis**

466 Significant differences in protein domain content annotated by InterProScan between the
467 compared genomes were identified using Fisher's exact test to calculate the *p-value* for the
468 difference in the number of InterPro domains between parmalean and diatom genomes. The *p-*
469 *values* were corrected for multiple comparisons using Bonferroni correction. For each genome,
470 protein sequences with 100% similarity to other genes were removed using CD-HIT (v.4.8.1)[108]
471 with the parameters -c 1 -aS 1.
472

473 **Predictions of phago-mixotrophy using a gene-based model**

474 Predicted protein data from eight parmalean genomes and five diatom genomes were tested
475 for phagocytotic potential using a gene-based model described by Burns et al[27]. To determine the
476 phagocytotic potential of parmaleans, we also tested the five transcriptomes of the naked flagellate
477 (bolidomonads) from the MMETSP database[79] and Kessenich et al. (2014)[109]. Gene annotation
478 was not available for the data from Kessenich et al. (2014)[109]; therefore, coding sequences were
479 annotated using TransDecoder (v.5.5.0) (https://github.com/TransDecoder/TransDecoder).
480

Phylogenetic analysis of silicon transporter domains

We used the sequence data of SIT proteins of diatoms and ochrophytes provided by Durkin et al. (2016)[50] in addition to those of parmaleans determined in this study. Diatom and parmalean SIT proteins are usually composed of a single SIT domain, but some contain more than two domains. To analyse multiple domains at once, SIT domain regions were determined using HMMER (v.3.3.2) with PF03842 from using the profile's GA gathering cutoff (--cut_ga mode) and selected for downstream analysis. Each SIT domain sequence was aligned using MAFFT (v.7.453) in the linsi mode and unreliable sequences were manually removed. A maximum likelihood phylogenetic tree was inferred from this multiple alignment using RAxML (v.8.2.12). The amino acid substitution model was automatically determined to be the LG model by the software. Bootstrap values were obtained based on 100 bootstrap replicates.

Phylogenetic analysis of plastocyanin

We used HmmerSearch (v.3.3) with TIGR02656.1 from TIGERFAMs using the profile's GA gathering cutoff (--cut_ga mode) to find plastocyanin genes in Uniref 90[78], MMETSP[79], and our genomes. The genes from MMETSP clustered with 97% similarity using CD-HIT (v.4.8.1). Unreliable sequences were removed manually. We next obtained 716 plastocyanin genes of photosynthetic eukaryotes, cyanobacteria, and cyanophages. Because of the large divergence of the sequences and small number of alignable regions, we used gs2, a software to conduct the Graph Splitting (GS) method[110], which can resolve the early evolution of protein families using a graph-based approach, to estimate the phylogenetic tree of plastocyanin. We ran the GS method with 100 replicates using the Edge Perturbation method for statistically evaluating branch reliability.

Data availability

Sequence data generated during the current study are available in DDBJ bioprojects, under accession number PRJDB14101 (RNA reads for *Triparma laevis* f. *inornata*), PRJDB13844 (DNA reads for the other seven strains), and PRJDB13933 (RNA reads for the other seven strains). The assembly data analysed during the current study are also available in the DDBJ repository, under accession numbers BLQM01000001-BLQM01000902 (*Triparma laevis* f. *inornata*), BRXW01000001-BRXW01001055 (*Triparma laevis* f. *longispina*),

BRXX01000001-BRXX01000659 (*Triparma verrucosa*), BRXY01000001-BRXY01000634 (*Triparma strigata*), BRXZ01000001-BRXZ01008760 (*Triparma retinervis*), BRYA01000001-BRYA01001858 (*Triparma colmacea*), BRYB01000001-BRYB01007082 (*Tetraparma gracilis*), and BRYC01000001-BRYC01001921 ('Scaly parma'). Data underlying Figs. and Supplementary Figs. are provided as Supplementary Data files.

Author Contributions

H.B. performed most of the bioinformatics analyses presented in this work and wrote initial version of the manuscript. R.B.-M., H.E., and H.O. supervised the bioinformatics part of the study. Y.N. performed genome assembly and gene prediction for *Triparma laevis* f. *inornata*. A.K. coordinated the genome sequencing part of the study. S.S., S.Y., K.Y., M.I., and A.K. contributed to culture and DNA/RNA sequencing. N.S. contributed to functional interpretation of the genomes. All authors contributed to the interpretation of the results and the finalization of the manuscript.

Competing interests statement

The authors declare no competing interests.

Acknowledgements

This work was supported by JSPS/KAKENHI (No. 22657027, 23370046, 26291085, 221S0002, 16K07489, 16H06279, 17H03724), the Canon Foundation, the Collaborative Research Program of Institute for Chemical Research, Kyoto University (No. 2016-30, 2015-39), and the JST "Establishment of University Fellowships Towards The Creation of Science Technology Innovation" Grant Number JPMJFS2123. Computational time was provided by the SuperComputer System, Institute for Chemical Research, Kyoto University. We thank Gabe Yedid, Ph.D., from Edanz (https://jp.edanz.com/english-editing-b) for editing a draft of this manuscript.

1. Booth, B. C. & Marchant, H. J. PARMALES, A NEW ORDER OF MARINE CHRYSOPHYTES, WITH DESCRIPTIONS OF THREE NEW GENERA AND SEVEN NEW SPECIES. *J. Phycol.* **23**, 245–260 (1987).
2. Ichinomiya, M. *et al.* Diversity and oceanic distribution of the Parmales (Bolidophyceae), a picoplanktonic group closely related to diatoms. *ISME J.* **10**, 2419–2434 (2016).
3. Kuwata, A. *et al.* Bolidophyceae, a Sister Picoplanktonic Group of Diatoms – A Review. *Front. Mar. Sci.* **5**, 370 (2018).
4. Hoshina, K., Uezato, Y. & Jordan, R. W. Parmales (Bolidophyceae) assemblages in the subarctic Pacific Ocean during the mid-1960s. *Phycologia* **60**, 35–47 (2021).
5. Ichinomiya, M. *et al.* ISOLATION AND CHARACTERIZATION OF PARMALES (HETEROKONTA/HETEROKONTOPHYTA/STRAMENOPILES) FROM THE OYASHIO REGION, WESTERN NORTH PACIFIC1: FIRST CHARACTERIZATION OF PARMALES. *J. Phycol.* **47**, 144–151 (2011).
6. Guillou, L. *et al.* BOLIDOMONAS: A NEW GENUS WITH TWO SPECIES BELONGING TO A NEW ALGAL CLASS, THE BOLIDOPHYCEAE (HETEROKONTA). *J. Phycol.* **35**, 368–381 (1999).
7. Mann, D. G. & Vanormelingen, P. An Inordinate Fondness? The Number, Distributions, and Origins of Diatom Species. *J. Eukaryot. Microbiol.* **60**, 414–420 (2013).
8. Behrenfeld, M. J. *et al.* Thoughts on the evolution and ecological niche of diatoms. *Ecol. Monogr.* **91**, (2021).
9. Litchman, E., Klausmeier, C. A., Schofield, O. M. & Falkowski, P. G. The role of functional traits and trade-offs in structuring phytoplankton communities: scaling from cellular to ecosystem level. *Ecol. Lett.* **10**, 1170–1181 (2007).

10. Mann, D. & Marchant, H. *The origins of the diatom and its life cycle*. vol. 38 (Clarendon Press, 1989).
11. Kooistra, W. H. C. F., Gersonde, R., Medlin, L. K. & Mann, D. G. The Origin and Evolution of the Diatoms: Their Adaptation to a Planktonic Existence. in *Evolution of Primary Producers in the Sea* 207–249 (Elsevier, 2007). doi:10.1016/B978-012370518-1/50012-6.
12. Drebes, G. Sexuality. *Sexuality.* 250–283 (1977).
13. Kuwata, A., Saitoh, K., Nakamura, Y., Ichinomiya, M. & Sato, N. Draft Whole-Genome Sequence of *Triparma laevis* f. *inornata* (Parmales, Bolidophyceae), Isolated from the Oyashio Region, Western North Pacific Ocean. *Microbiol. Resour. Announc.* **9**, (2020).
14. Konno, S., Ohira, R., Komuro, C., Harada, N. & Jordan, R. W. Six new taxa of subarctic Parmales (Chrysophyceae). *J. Nannoplankton Res.* **29**, 108–128 (2007).
15. Armbrust, E. V. *et al.* The Genome of the Diatom *Thalassiosira Pseudonana* : Ecology, Evolution, and Metabolism. *Science* **306**, 79–86 (2004).
16. Bowler, C. *et al.* The Phaeodactylum genome reveals the evolutionary history of diatom genomes. *Nature* **456**, 239–244 (2008).
17. Basu, S. *et al.* Finding a partner in the ocean: molecular and evolutionary bases of the response to sexual cues in a planktonic diatom. *New Phytol.* **215**, 140–156 (2017).
18. Berges, J. A. & Falkowski, P. G. Physiological stress and cell death in marine phytoplankton: Induction of proteases in response to nitrogen or light limitation. *Limnol. Oceanogr.* **43**, 129–135 (1998).
19. Allen, A. E. *et al.* Whole-cell response of the pennate diatom Phaeodactylum tricornutum to iron starvation. *Proc. Natl. Acad. Sci.* **105**, 10438–10443 (2008).

20. Gallo, C., d'Ippolito, G., Nuzzo, G., Sardo, A. & Fontana, A. Autoinhibitory sterol sulfates mediate programmed cell death in a bloom-forming marine diatom. *Nat. Commun.* **8**, 1292 (2017).
21. Fu, W. *et al.* GPCR Genes as Activators of Surface Colonization Pathways in a Model Marine Diatom. *iScience* **23**, 101424 (2020).
22. Taylor, A. R. A Fast Na+/Ca2+-Based Action Potential in a Marine Diatom. *PLoS ONE* **4**, e4966 (2009).
23. Helliwell, K. E. *et al.* Alternative Mechanisms for Fast Na+/Ca2+ Signaling in Eukaryotes via a Novel Class of Single-Domain Voltage-Gated Channels. *Curr. Biol.* **29**, 1503-1511.e6 (2019).
24. Helliwell, K. E. *et al.* Spatiotemporal patterns of intracellular Ca^{2+} signalling govern hypo-osmotic stress resilience in marine diatoms. *New Phytol.* **230**, 155–170 (2021).
25. Lung, S.-C. & Weselake, R. J. Diacylglycerol acyltransferase: A key mediator of plant triacylglycerol synthesis. *Lipids* **41**, 1073–1088 (2006).
26. Alpy, F. & Tomasetto, C. Give lipids a START: the StAR-related lipid transfer (START) domain in mammals. *J. Cell Sci.* **118**, 2791–2801 (2005).
27. Burns, J. A., Pittis, A. A. & Kim, E. Gene-based predictive models of trophic modes suggest Asgard archaea are not phagocytotic. *Nat. Ecol. Evol.* **2**, 697–704 (2018).
28. Cougoule, C., Wiedemann, A., Lim, J. & Caron, E. Phagocytosis, an alternative model system for the study of cell adhesion. *Semin. Cell Dev. Biol.* **15**, 679–689 (2004).
29. Groves, E., Dart, A. E., Covarelli, V. & Caron, E. Molecular mechanisms of phagocytic uptake in mammalian cells. *Cell. Mol. Life Sci.* **65**, 1957–1976 (2008).

30. May, R. C. & Machesky, L. M. Phagocytosis and the actin cytoskeleton. *J. Cell Sci.* **114**, 1061–1077 (2001).

31. Zimmerli, S. *et al.* Phagosome-lysosome fusion is a calcium-independent event in macrophages. *J. Cell Biol.* **132**, 49–61 (1996).

32. Buckley, C. M. *et al.* WASH drives early recycling from macropinosomes and phagosomes to maintain surface phagocytic receptors. *Proc. Natl. Acad. Sci.* **113**, E5906–E5915 (2016).

33. Frias-Lopez, J., Thompson, A., Waldbauer, J. & Chisholm, S. W. Use of stable isotope-labelled cells to identify active grazers of picocyanobacteria in ocean surface waters. *Environ. Microbiol.* **11**, 512–525 (2009).

34. Li, Q., Edwards, K. F., Schvarcz, C. R. & Steward, G. F. Broad phylogenetic and functional diversity among mixotrophic consumers of Prochlorococcus. *ISME J.* **16**, 1557–1569 (2022).

35. van Dam, T. J. P. *et al.* Evolution of modular intraflagellar transport from a coatomer-like progenitor. *Proc. Natl. Acad. Sci.* **110**, 6943–6948 (2013).

36. Yamada, K. *et al.* Mitotic spindle formation in Triparma laevis NIES-2565(Parmales, Heterokontophyta). *Protoplasma* **254**, 461–471 (2017).

37. Moore, E. R. *et al.* Morphological and transcriptomic evidence for ammonium induction of sexual reproduction in Thalassiosira pseudonana and other centric diatoms. *PLOS ONE* **12**, e0181098 (2017).

38. Chepurnov, V. A., Mann, D. G., Sabbe, K. & Vyverman, W. Experimental Studies on Sexual Reproduction in Diatoms. in *International Review of Cytology* vol. 237 91–154 (Elsevier, 2004).

623 39. Jensen, K. G., Moestrup, Ø. & Schmid, A.-M. M. Ultrastructure of the male gametes from
624 two centric diatoms, Chaetoceros laciniosus and Coscinodiscus wailesii (Bacillariophyceae).
625 *Phycologia* **42**, 98–105 (2003).
626 40. Schreiber, V. *et al.* The Central Vacuole of the Diatom Phaeodactylum tricornutum :
627 Identification of New Vacuolar Membrane Proteins and of a Functional Di-leucine-based
628 Targeting Motif. *Protist* **168**, 271–282 (2017).
629 41. Horák, A., Allen, A. E. & Oborník, M. Common origin of ornithine–urea cycle in
630 opisthokonts and stramenopiles. *Sci. Rep.* **10**, 16687 (2020).
631 42. Dong, H.-P. *et al.* Understanding Strategy of Nitrate and Urea Assimilation in a Chinese
632 Strain of Aureococcus anophagefferens through RNA-Seq Analysis. *PLoS ONE* **9**, e111069
633 (2014).
634 43. Smith, S. R. *et al.* Evolution and regulation of nitrogen flux through compartmentalized
635 metabolic networks in a marine diatom. *Nat. Commun.* **10**, 4552 (2019).
636 44. Behrenfeld, M. J., Bale, A. J., Kolber, Z. S., Aiken, J. & Falkowski, P. G. Confirmation of
637 iron limitation of phytoplankton photosynthesis in the equatorial Pacific Ocean. *Nature* **383**,
638 508–511 (1996).
639 45. Severance, S., Chakraborty, S. & Kosman, D. J. The Ftr1p iron permease in the yeast plasma
640 membrane: orientation, topology and structure-function relationships. *Biochem. J.* **380**, 487–
641 496 (2004).
642 46. Morrissey, J. *et al.* A Novel Protein, Ubiquitous in Marine Phytoplankton, Concentrates Iron
643 at the Cell Surface and Facilitates Uptake. *Curr. Biol.* **25**, 364–371 (2015).
644 47. Kazamia, E. *et al.* Endocytosis-mediated siderophore uptake as a strategy for Fe acquisition
645 in diatoms. *Sci. Adv.* **4**, eaar4536 (2018).

646 48. Peers, G. & Price, N. M. Copper-containing plastocyanin used for electron transport by an
647 oceanic diatom. *Nature* **441**, 341–344 (2006).
648 49. Groussman, R. D., Parker, M. S. & Armbrust, E. V. Diversity and Evolutionary History of
649 Iron Metabolism Genes in Diatoms. *PLOS ONE* **10**, e0129081 (2015).
650 50. Durkin, C. A., Koester, J. A., Bender, S. J. & Armbrust, E. V. The evolution of silicon
651 transporters in diatoms. *J. Phycol.* **52**, 716–731 (2016).
652 51. Kotzsch, A. *et al.* Silicanin-1 is a conserved diatom membrane protein involved in silica
653 biomineralization. *BMC Biol.* **15**, 65 (2017).
654 52. Poulsen, N. & Kröger, N. Silica Morphogenesis by Alternative Processing of Silaffins in the
655 Diatom Thalassiosira pseudonana. *J. Biol. Chem.* **279**, 42993–42999 (2004).
656 53. Wenzl, S., Hett, R., Richthammer, P. & Sumper, M. Silacidins: Highly Acidic
657 Phosphopeptides from Diatom Shells Assist in Silica Precipitation In Vitro. *Angew. Chem.*
658 *Int. Ed.* **47**, 1729–1732 (2008).
659 54. Scheffel, A., Poulsen, N., Shian, S. & Kroger, N. Nanopatterned protein microrings from a
660 diatom that direct silica morphogenesis. *Proc. Natl. Acad. Sci.* **108**, 3175–3180 (2011).
661 55. Kotzsch, A. *et al.* Biochemical Composition and Assembly of Biosilica-associated Insoluble
662 Organic Matrices from the Diatom Thalassiosira pseudonana. *J. Biol. Chem.* **291**, 4982–4997
663 (2016).
664 56. Flynn, K. J. & Mitra, A. Building the 'perfect beast': modelling mixotrophic plankton. *J.*
665 *Plankton Res.* **31**, 965–992 (2009).
666 57. Ward, B. A., Dutkiewicz, S., Barton, A. D. & Follows, M. J. Biophysical Aspects of
667 Resource Acquisition and Competition in Algal Mixotrophs. *Am. Nat.* **178**, 98–112 (2011).

668 58. Troost, T. A., Kooi, B. W. & Kooijman, S. A. L. M. When do mixotrophs specialize?
669 Adaptive dynamics theory applied to a dynamic energy budget model. *Math. Biosci.* **193**,
670 159–182 (2005).
671 59. Troost, T. A., Kooi, B. W. & Kooijman, S. A. L. M. Ecological Specialization of
672 Mixotrophic Plankton in a Mixed Water Column. *Am. Nat.* **166**, E45–E61 (2005).
673 60. Endo, H., Ogata, H. & Suzuki, K. Contrasting biogeography and diversity patterns between
674 diatoms and haptophytes in the central Pacific Ocean. *Sci. Rep.* **8**, 10916 (2018).
675 61. Xu, Z. *et al.* Disentangling the Ecological Processes Shaping the Latitudinal Pattern of
676 Phytoplankton Communities in the Pacific Ocean. *mSystems* **7**, e01203-21 (2022).
677 62. Houdan, A., Probert, I., Zatylny, C., Véron, B. & Billard, C. Ecology of oceanic
678 coccolithophores. I. Nutritional preferences of the two stages in the life cycle of Coccolithus
679 braarudii and Calcidiscus leptoporus. *Aquat. Microb. Ecol.* **44**, 291–301 (2006).
680 63. Innan, H. & Kondrashov, F. The evolution of gene duplications: classifying and
681 distinguishing between models. *Nat. Rev. Genet.* **11**, 97–108 (2010).
682 64. Reinfelder, J. R. Carbon Concentrating Mechanisms in Eukaryotic Marine Phytoplankton.
683 *Annu. Rev. Mar. Sci.* **3**, 291–315 (2011).
684 65. Stoecker, D. K., Hansen, P. J., Caron, D. A. & Mitra, A. Mixotrophy in the Marine Plankton.
685 *Annu. Rev. Mar. Sci.* **9**, 311–335 (2017).
686 66. Medlin, L. K. A Review of the Evolution of the Diatoms from the Origin of the Lineage to
687 Their Populations. in *The Diatom World* (eds. Seckbach, J. & Kociolek, P.) vol. 19 93–118
688 (Springer Netherlands, 2011).

689 67. Winter, C., Bouvier, T., Weinbauer, M. G. & Thingstad, T. F. Trade-Offs between
690 Competition and Defense Specialists among Unicellular Planktonic Organisms: the "Killing
691 the Winner" Hypothesis Revisited. *Microbiol. Mol. Biol. Rev.* **74**, 42–57 (2010).
692 68. Kröger, N., Deutzmann, R., Bergsdorf, C. & Sumper, M. Species-specific polyamines from
693 diatoms control silica morphology. *Proc. Natl. Acad. Sci.* **97**, 14133–14138 (2000).
694 69. Boyd, P. W. *et al.* Mesoscale Iron Enrichment Experiments 1993-2005: Synthesis and Future
695 Directions. *Science* **315**, 612–617 (2007).
696 70. Boiteau, R. M. *et al.* Siderophore-based microbial adaptations to iron scarcity across the
697 eastern Pacific Ocean. *Proc. Natl. Acad. Sci.* **113**, 14237–14242 (2016).
698 71. Guillard, R. R. L. & Ryther, J. H. STUDIES OF MARINE PLANKTONIC DIATOMS: I.
699 CYCLOTELLA NANA HUSTEDT, AND DETONULA CONFERVACEA (CLEVE)
700 GRAN. *Can. J. Microbiol.* **8**, 229–239 (1962).
701 72. Bolger, A. M., Lohse, M. & Usadel, B. Trimmomatic: a flexible trimmer for Illumina
702 sequence data. *Bioinformatics* **30**, 2114–2120 (2014).
703 73. Kajitani, R. *et al.* Efficient de novo assembly of highly heterozygous genomes from whole-
704 genome shotgun short reads. *Genome Res.* **24**, 1384–1395 (2014).
705 74. Li, H. & Durbin, R. Fast and accurate short read alignment with Burrows-Wheeler transform.
706 *Bioinformatics* **25**, 1754–1760 (2009).
707 75. Sims, D. *et al.* CGAT: computational genomics analysis toolkit. *Bioinformatics* **30**, 1290–
708 1291 (2014).
709 76. Besemer, J. GeneMarkS: a self-training method for prediction of gene starts in microbial
710 genomes. Implications for finding sequence motifs in regulatory regions. *Nucleic Acids Res.*
711 **29**, 2607–2618 (2001).

712 77. Carradec, Q. *et al.* A global ocean atlas of eukaryotic genes. *Nat. Commun.* **9**, 373 (2018).
713 78. Suzek, B. E. *et al.* UniRef clusters: a comprehensive and scalable alternative for improving
714 sequence similarity searches. *Bioinformatics* **31**, 926–932 (2015).
715 79. Keeling, P. J. *et al.* The Marine Microbial Eukaryote Transcriptome Sequencing Project
716 (MMETSP): Illuminating the Functional Diversity of Eukaryotic Life in the Oceans through
717 Transcriptome Sequencing. *PLoS Biol.* **12**, e1001889 (2014).
718 80. Mihara, T. *et al.* Linking Virus Genomes with Host Taxonomy. *Viruses* **8**, 66 (2016).
719 81. Buchfink, B., Xie, C. & Huson, D. H. Fast and sensitive protein alignment using
720 DIAMOND. *Nat. Methods* **12**, 59–60 (2015).
721 82. Herath, D., Tang, S.-L., Tandon, K., Ackland, D. & Halgamuge, S. K. CoMet: a workflow
722 using contig coverage and composition for binning a metagenomic sample with high
723 precision. *BMC Bioinformatics* **18**, 571 (2017).
724 83. Tajima, N. *et al.* Sequencing and analysis of the complete organellar genomes of Parmales, a
725 closely related group to Bacillariophyta (diatoms). *Curr. Genet.* **62**, 887–896 (2016).
726 84. Lowe, T. M. & Eddy, S. R. tRNAscan-SE: A Program for Improved Detection of Transfer
727 RNA Genes in Genomic Sequence. *Nucleic Acids Res.* **25**, 955–964 (1997).
728 85. Stanke, M., Diekhans, M., Baertsch, R. & Haussler, D. Using native and syntenically
729 mapped cDNA alignments to improve de novo gene finding. *Bioinformatics* **24**, 637–644
730 (2008).
731 86. Kim, D. *et al.* TopHat2: accurate alignment of transcriptomes in the presence of insertions,
732 deletions and gene fusions. *Genome Biol.* **14**, R36 (2013).

733 87. Trapnell, C. *et al.* Transcript assembly and quantification by RNA-Seq reveals unannotated
734 transcripts and isoform switching during cell differentiation. *Nat. Biotechnol.* **28**, 511–515
735 (2010).
736 88. Haas, B. J. *et al.* De novo transcript sequence reconstruction from RNA-seq using the Trinity
737 platform for reference generation and analysis. *Nat. Protoc.* **8**, 1494–1512 (2013).
738 89. Slater, G. & Birney, E. Automated generation of heuristics for biological sequence
739 comparison. *BMC Bioinformatics* **6**, 31 (2005).
740 90. Chan, P. P., Lin, B. Y., Mak, A. J. & Lowe, T. M. *tRNAscan-SE 2.0: Improved Detection*
741 *and Functional Classification of Transfer RNA Genes*.
742 http://biorxiv.org/lookup/doi/10.1101/614032 (2019) doi:10.1101/614032.
743 91. Nawrocki, E. P. & Eddy, S. R. Infernal 1.1: 100-fold faster RNA homology searches.
744 *Bioinformatics* **29**, 2933–2935 (2013).
745 92. Flynn, J. M. *et al.* RepeatModeler2 for automated genomic discovery of transposable
746 element families. *Proc. Natl. Acad. Sci.* **117**, 9451–9457 (2020).
747 93. Tarailo-Graovac, M. & Chen, N. Using RepeatMasker to Identify Repetitive Elements in
748 Genomic Sequences. *Curr. Protoc. Bioinforma.* **25**, (2009).
749 94. Brůna, T., Hoff, K. J., Lomsadze, A., Stanke, M. & Borodovsky, M. BRAKER2: automatic
750 eukaryotic genome annotation with GeneMark-EP+ and AUGUSTUS supported by a protein
751 database. *NAR Genomics Bioinforma.* **3**, lqaa108 (2021).
752 95. Kriventseva, E. V. *et al.* OrthoDB v10: sampling the diversity of animal, plant, fungal,
753 protist, bacterial and viral genomes for evolutionary and functional annotations of orthologs.
754 *Nucleic Acids Res.* **47**, D807–D811 (2019).

755 96. Dobin, A. *et al.* STAR: ultrafast universal RNA-seq aligner. *Bioinformatics* **29**, 15–21
756 (2013).
757 97. Jones, P. *et al.* InterProScan 5: genome-scale protein function classification. *Bioinformatics*
758 **30**, 1236–1240 (2014).
759 98. Huerta-Cepas, J. *et al.* Fast Genome-Wide Functional Annotation through Orthology
760 Assignment by eggNOG-Mapper. *Mol. Biol. Evol.* **34**, 2115–2122 (2017).
761 99. Huerta-Cepas, J. *et al.* eggNOG 5.0: a hierarchical, functionally and phylogenetically
762 annotated orthology resource based on 5090 organisms and 2502 viruses. *Nucleic Acids Res.*
763 **47**, D309–D314 (2019).
764 100. Fukasawa, Y. *et al.* MitoFates: Improved Prediction of Mitochondrial Targeting
765 Sequences and Their Cleavage Sites*. *Mol. Cell. Proteomics* **14**, 1113–1126 (2015).
766 101. Almagro Armenteros, J. J. *et al.* Detecting sequence signals in targeting peptides using
767 deep learning. *Life Sci. Alliance* **2**, e201900429 (2019).
768 102. Nielsen, H. Predicting Secretory Proteins with SignalP. in *Protein Function Prediction*
769 (ed. Kihara, D.) vol. 1611 59–73 (Springer New York, 2017).
770 103. Gruber, A., Rocap, G., Kroth, P. G., Armbrust, E. V. & Mock, T. Plastid proteome
771 prediction for diatoms and other algae with secondary plastids of the red lineage. *Plant J.* **81**,
772 519–528 (2015).
773 104. Emms, D. M. & Kelly, S. OrthoFinder: phylogenetic orthology inference for
774 comparative genomics. *Genome Biol.* **20**, 238 (2019).
775 105. Katoh, K. & Standley, D. M. MAFFT Multiple Sequence Alignment Software Version
776 7: Improvements in Performance and Usability. *Mol. Biol. Evol.* **30**, 772–780 (2013).

106. Capella-Gutierrez, S., Silla-Martinez, J. M. & Gabaldon, T. trimAl: a tool for automated alignment trimming in large-scale phylogenetic analyses. *Bioinformatics* **25**, 1972–1973 (2009).

107. Stamatakis, A. RAxML version 8: a tool for phylogenetic analysis and post-analysis of large phylogenies. *Bioinformatics* **30**, 1312–1313 (2014).

108. Li, W. & Godzik, A. Cd-hit: a fast program for clustering and comparing large sets of protein or nucleotide sequences. *Bioinformatics* **22**, 1658–1659 (2006).

109. Kessenich, C. R., Ruck, E. C., Schurko, A. M., Wickett, N. J. & Alverson, A. J. Transcriptomic Insights into the Life History of Bolidophytes, the Sister Lineage to Diatoms. *J. Phycol.* **50**, 977–983 (2014).

110. Matsui, M. & Iwasaki, W. Graph Splitting: A Graph-Based Approach for Superfamily-Scale Phylogenetic Tree Reconstruction. *Syst. Biol.* syz049 (2019) doi:10.1093/sysbio/syz049.

111. Jensen, E. L., Maberly, S. C. & Gontero, B. Insights on the Functions and Ecophysiological Relevance of the Diverse Carbonic Anhydrases in Microalgae. *Int. J. Mol. Sci.* **21**, 2922 (2020).

794 Table 1 Assembly and annotation results and statistics

795

	Triparma laevis f. inornata	*Triparma laevis* f. *longispina*	*Triparma verrucosa*	*Triparma strigata*	*Triparma retinervis*	*Triparma colmacea*	*Tetraparma gracilis*	Scaly parma
Genome size (Mbp)	42.6	41.4	35.5	35.2	36.5	43.0	43.6	31.0
No. of scaffolds	902	1,055	659	634	8,760	1,858	7,082	1,921
N50 (kbp)	83.2	77.9	74.0	73.4	8.2	63.5	10.7	51.7
GC (%)	51.3	51.1	52.1	52.2	52.4	51.0	64.8	51.0
No. of predicted protein-coding genes	13,396	16,002	14,488	14,364	13,636	13,919	15,310	12,177
BUSCO Complete genes (%)	74	93	94	94	70	92	65	93

Figure legends

Fig. 1 | Phylogenetic relationships of diatoms, parmaleans (Parmales), and stramenopiles, and number of shared genes in OGs.

(a) Maximum likelihood tree estimated by RAxML with 164 single-copy OGs. Blue and purple branches are diatom and Parmales clades, respectively. The numbers on the branches represent bootstrap values. The coloured bars indicate the group where each taxon belongs (black: outgroup, light blue: pennate diatoms, deep blue: centric diatoms, purple: Parmales). (b) The barplot represents the groups genes inferred through orthologous gene clustering.

Fig. 2

(a) Diatom and Parmales genomes enriched in InterPro domains. We manually clustered and selected the domains that appear to be involved in a specific process. The colours are scaled in ascending order from blue to red by the z-value in each row. (b) Number of genes annotated with GO:0005516 (calcium ion binding) by InterProScan. (c) An example of InterPro domains composed of multi-domain proteins including START domains. (d) Parmalean genomes enriched in InterPro domains thought to be related to phagocytosis. The colours are scaled in ascending order from blue to red by the z-value in each row. InterPro domains that were not statistically significant but were considered important are marked with an asterisk (*). (e) Probability of phagotrophy predicted by the Burns et al. (2019) tool. (f) Schematic view of hypothesized parmalean life cycle. (g) Presence (filled square) or absence (or loss: grey square) of genes/transcripts related to intraflagellar transport (IFT) subunits.

Fig. 3 | Ecophysiology of diatoms and parmaleans.

(a) Distribution of nutrient transporter genes. Each axis represents the number of nitrate/nitrite transporter, ammonia transporter, urea transporter, phosphate transporter, or silicic acid (Si) transporter genes. (b) Genes involved in nitrogen assimilation (including ornithine–urea cycle). The colours are scaled in ascending order from blue to red by the z-value in each row; a grey square indicates absence of the gene. (c) Presence (filled square) or absence/loss (grey square) of iron uptake system genes. Gene names are abbreviated; full names and accessions can be found

825 in Supplementary Data 4. (d) Schematic view of the evolutionary pattern of plastocyanin genes. A
826 whole phylogenetic tree is shown in Supplementary Fig. 3.
827
828 Fig. 4 | Phylogenetic tree of SIT domains.
829 Maximum likelihood phylogenetic tree of the SIT domains of diatoms, Parmales, and
830 ochrophytes (outgroup). Sequences with more than two SIT domains were separated to each
831 domain and aligned. Grouping of paralogues from diatoms is based on the classification of Durkin
832 et al. (2016). Only important bootstrap values are noted.
833
834 Fig. 5 | Schematic view of diatoms and parmales evolution.

835 **Figure 1**

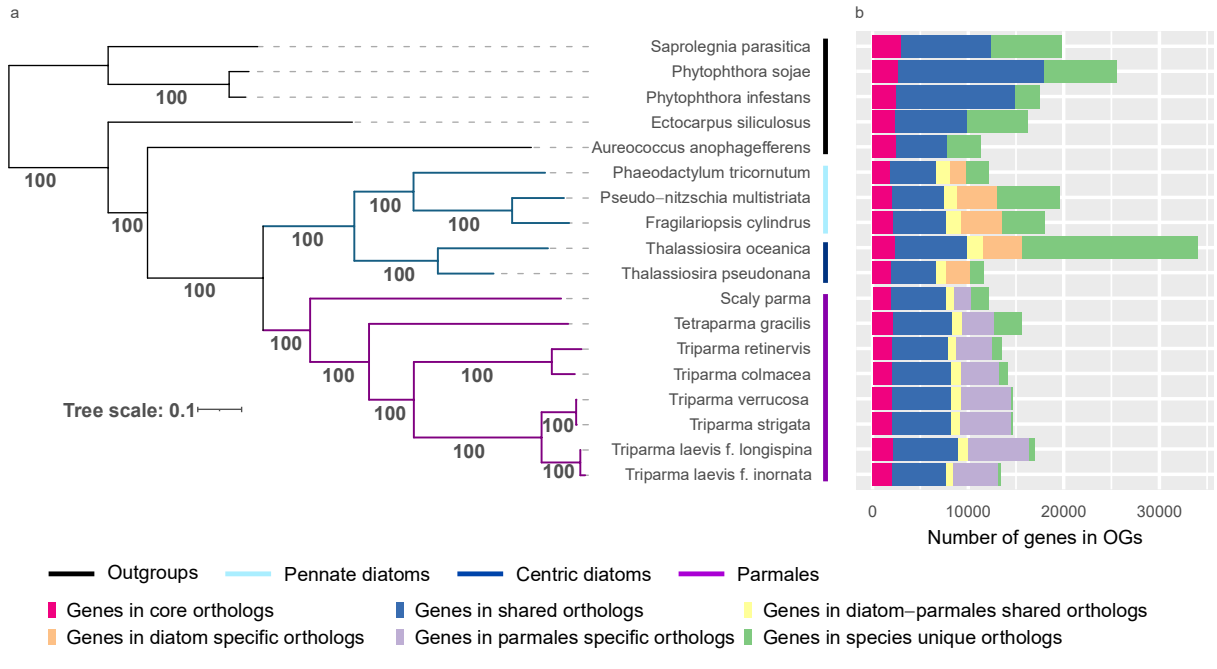

836

Figure. 2

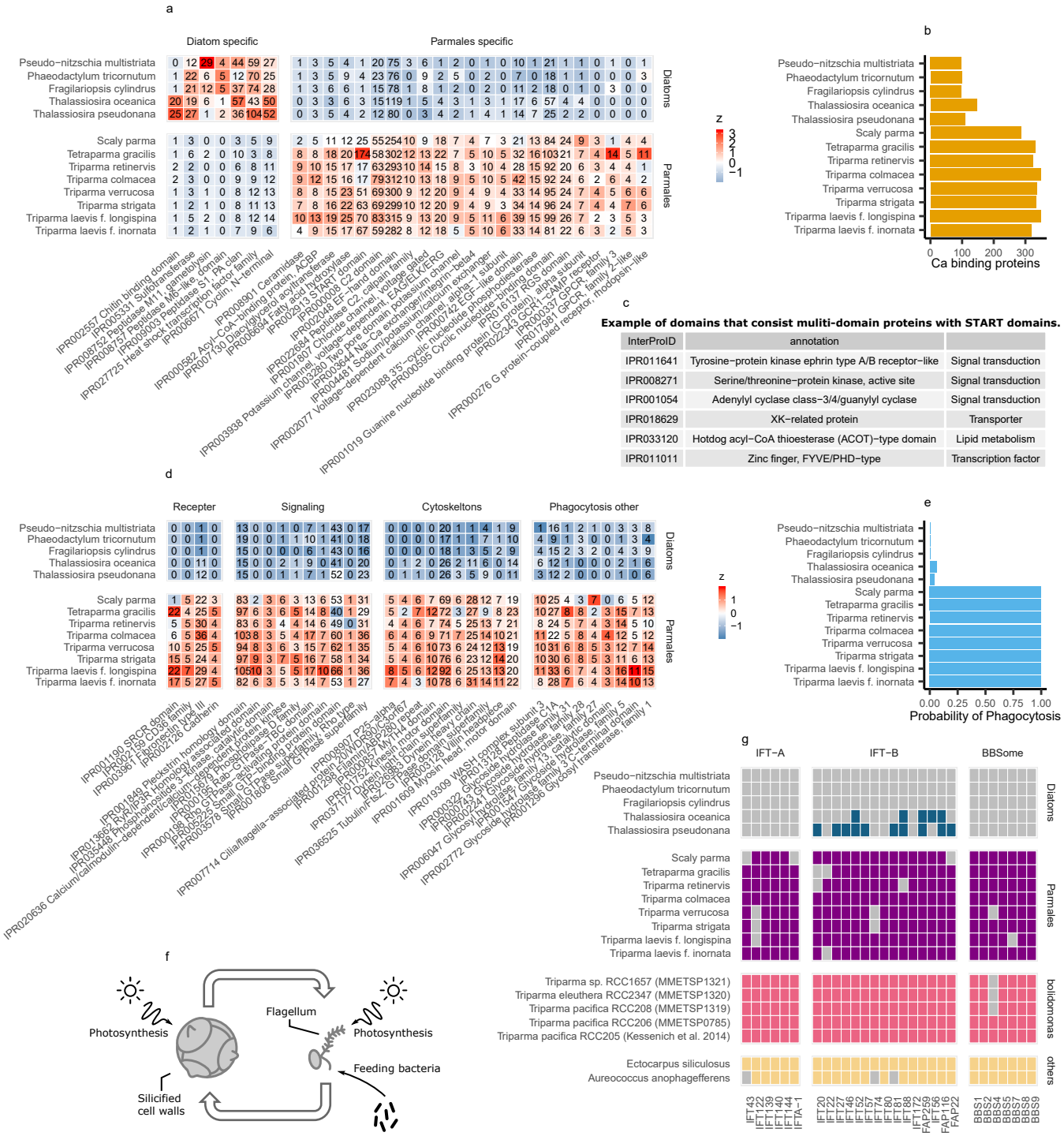

Figure. 3

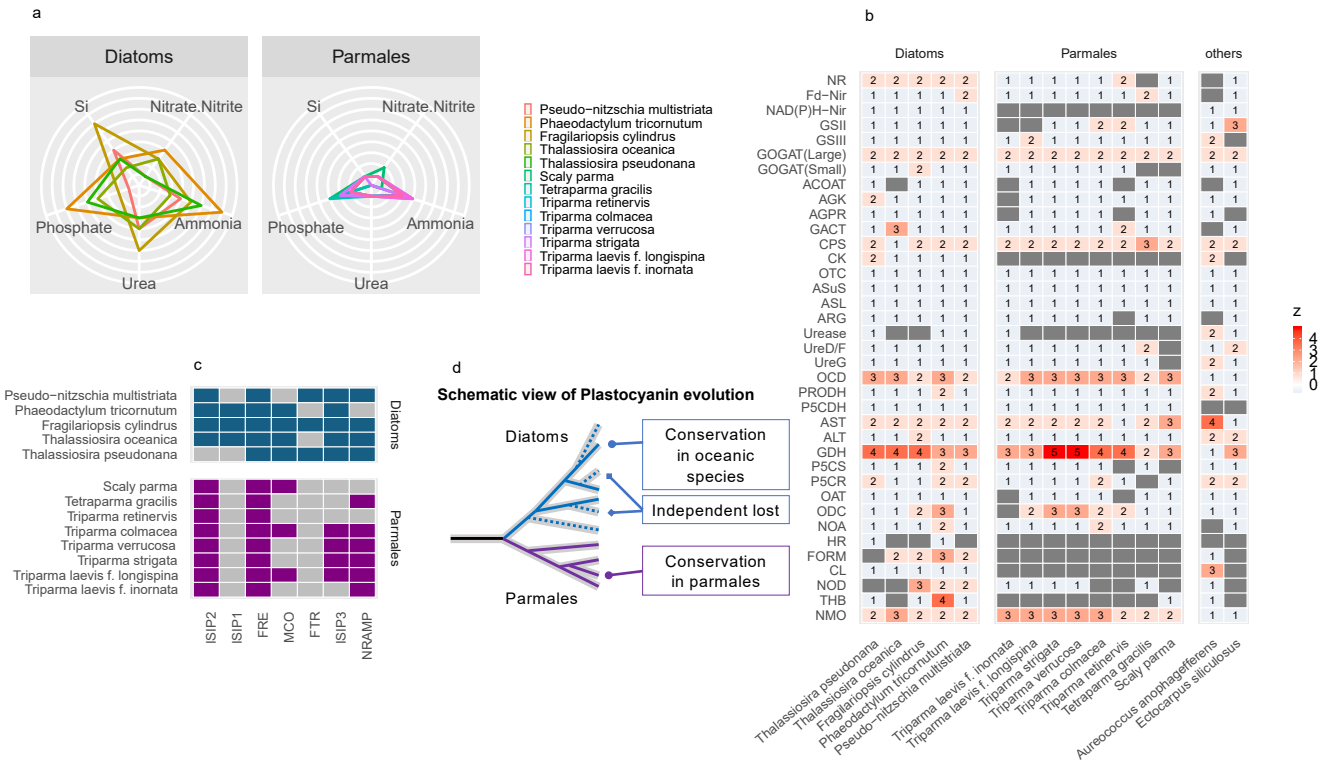

841 **Figure 4**

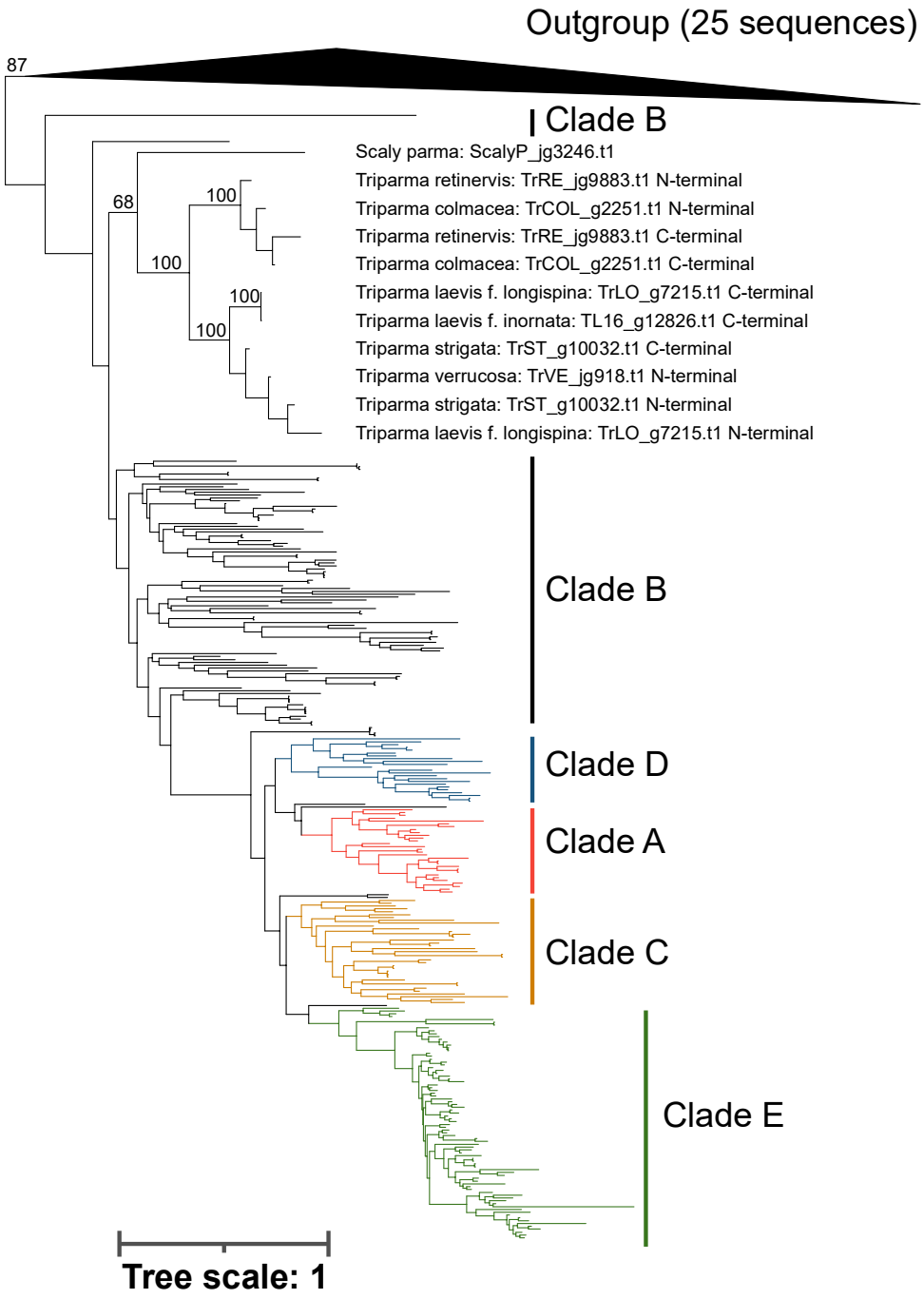

842

Figure. 5